

# Journal of Biomedical Optics

BiomedicalOptics.SPIEDigitalLibrary.org

## **Noninvasive assessment of articular cartilage surface damage using reflected polarized light microscopy**

Ruby N. Huynh  
George Nehmetallah  
Christopher B. Raub

**SPIE.**

Ruby N. Huynh, George Nehmetallah, Christopher B. Raub, "Noninvasive assessment of articular cartilage surface damage using reflected polarized light microscopy," *J. Biomed. Opt.* **22**(6), 065001 (2017), doi: 10.1117/1.JBO.22.6.065001.

# Noninvasive assessment of articular cartilage surface damage using reflected polarized light microscopy

Ruby N. Huynh,<sup>a</sup> George Nehmetallah,<sup>b</sup> and Christopher B. Raub<sup>a,\*</sup>

<sup>a</sup>The Catholic University of America, Department of Biomedical Engineering, Washington, United States

<sup>b</sup>The Catholic University of America, Department of Electrical Engineering, Washington, United States

**Abstract.** Articular surface damage occurs to cartilage during normal aging, osteoarthritis, and in trauma. A noninvasive assessment of cartilage microstructural alterations is useful for studies involving cartilage explants. This study evaluates polarized reflectance microscopy as a tool to assess surface damage to cartilage explants caused by mechanical scraping and enzymatic degradation. Adult bovine articular cartilage explants were scraped, incubated in collagenase, or underwent scrape and collagenase treatments. In an additional experiment, cartilage explants were subject to scrapes at graduated levels of severity. Polarized reflectance parameters were compared with India ink surface staining, features of histological sections, changes in explant wet weight and thickness, and chondrocyte viability. The polarized reflectance signal was sensitive to surface scrape damage and revealed individual scrape features consistent with India ink marks. Following surface treatments, the reflectance contrast parameter was elevated and correlated with image area fraction of India ink. After extensive scraping, polarized reflectance contrast and chondrocyte viability were lower than that from untreated explants. As part of this work, a mathematical model was developed and confirmed the trend in the reflectance signal due to changes in surface scattering and subsurface birefringence. These results demonstrate the effectiveness of polarized reflectance microscopy to sensitively assess surface microstructural alterations in articular cartilage explants. © 2017 Society of Photo-Optical Instrumentation Engineers (SPIE) [DOI: 10.1117/1.JBO.22.6.065001]

Keywords: polarization; reflectance; microscopy; surfaces; articular cartilage.

Paper 170052RR received Jan. 19, 2017; accepted for publication May 15, 2017; published online Jun. 5, 2017.

## 1 Introduction

Articular cartilage surfaces play a vital role in load distribution and friction reduction of knee joints during movement.<sup>1</sup> Mechanical load is distributed through a distinct zonal architecture in articular cartilage,<sup>2</sup> consisting of type II collagen and glycosaminoglycans.<sup>3–5</sup> In the superficial zone, collagen microstructure is tangential to the articular surface and accounts for 60% to 86% of dry weight of that layer.<sup>6,7</sup> Minimal fibrillation is usually apparent in this layer in normal aging.<sup>6,8</sup> Additionally, in osteoarthritis, alterations to the superficial zone become larger progressively with disease stage.<sup>6</sup> Therefore, noninvasive optical detection of mild microstructural alterations to the superficial zone is of interest to orthopedic researchers seeking to identify causes and patterns of damage to the articular surface and superficial zone. Identification of microstructural alterations without staining the articular surface would be useful for *in vitro* studies of progressive cartilage damage and remodeling.

Bovine articular cartilage explants are useful in *in vitro* models to determine cartilage microstructural and chondrocyte responses to mechanical loading,<sup>9,10</sup> growth conditions,<sup>11–13</sup> degradation,<sup>14</sup> and degeneration.<sup>15,16</sup> The effects of injurious mechanical treatments include death of chondrocytes and suppression of glycosaminoglycan synthesis.<sup>9,10</sup> Several *in vitro* treatments, including soluble factors, such as IGF-1, TGF- $\beta$ 1, BMP-7, and PDGF-AB,<sup>12</sup> and enzymes such as chondroitinase ABC<sup>11,13</sup> influence the rate and quality of cartilage tissue growth by modulating the mass balance of collagen and

glycosaminoglycans. Enzymatic degradation of cartilage explants with collagenase initially produces tissue swelling as the collagen network is compromised and leads to tissue loss with further collagenase activity.<sup>14</sup> The effects of proinflammatory factors, such as TNF- $\alpha$ , IL-1 $\alpha$ , and IL-1 $\beta$ , on explants include collagen degradation but also stimulation of factors related to collagen anabolism such as BMP-2.<sup>16</sup> A nondamaging technique that assesses some aspects of cartilage microstructure could reveal responses to these treatments, in the same explant, over multiple time points during culture.

Several optical techniques assess microstructural alterations in bovine cartilage explants. Optical coherence tomography (OCT) detects clefts, cracks, and fibrillated articular surfaces, as well as the entire cartilage thickness by depth-resolved backscattering from tissue interfaces.<sup>17</sup> Visible wavelength multispectral imaging<sup>14</sup> and fluorescence spectroscopy<sup>18</sup> are two additional tools to assess cartilage surfaces and can distinguish normal and mechanically or enzymatically degraded cartilage from bovine knee joints. In addition, healthy bovine articular cartilage examined by two-photon laser scanning microscopy (TPLSM) reveals two photon fluorescence and second harmonic generation signals deriving from endogenous fluorophores in chondrocytes and type II collagen, respectively.<sup>19</sup> It is important to note that the extent of mild surface damage features, termed minimal fibrillation, is not readily apparent macroscopically or with conventional microscopes without staining.<sup>20</sup> Marking the articular surface with India ink reveals contrast between minimally fibrillated and smooth articular surfaces but is not compatible with

\*Address all correspondence to: Christopher B. Raub, E-mail: [raubc@cua.edu](mailto:raubc@cua.edu)

long-term explant culture or intravital staining. Furthermore, the long-term effects of repeated laser irradiation on cells and tissue are not clear. Hence, there is a need for a safe, noninvasive, label-free method to assess the articular surface, to better track microstructural alterations in cartilage explants during *in vitro* culture.

Depth-resolved optical tomographic and three-dimensional (3-D) imaging techniques are sensitive to microscale articular surface damage and as well as subsurface alterations. While OCT, with a resolution of  $\sim 5 \mu\text{m}$ , detects mild alterations to the articular surface,<sup>21</sup> tomographic acquisition typically avoids large surface coverage.<sup>21,22</sup> Polarization-sensitive OCT is sensitive to collagen birefringence in articular cartilage, relaying information about the collagen network microstructure throughout the tomographic section.<sup>21,23</sup> In contrast, TPLSM produces *en face* images of cartilage to a depth of several hundreds of microns and can track altered collagen microstructure as well as chondrocyte location beneath the articular surface.<sup>24</sup> Since cartilage is a highly scattering tissue, depth-resolved techniques, such as OCT and TPLSM, provide significant subsurface details.<sup>25–27</sup> However, particularly in cartilage explant studies involving the articular surface, a rapid, noninvasive optical technique requiring lower light fluence in the tissue would ensure chondrocyte viability during repetitive imaging.

Polarized light transmittance and reflectance reveal characteristics of thin/transparent<sup>28,29</sup> and thick/opaque tissues,<sup>30–32</sup> respectively. In transmission through a transverse slide section, three distinct zones of collagen alignment are apparent: the superficial zone, with tangential alignment, the isotropic middle zone, and the deep zone with perpendicular alignment to the articular surface.<sup>33,34</sup> In contrast to transmission techniques, polarized reflectance microscopy from articular cartilage has been less reported. Interactions of polarized light in biological tissues include multiple scattering, dichroism, optical rotation, and linear birefringence.<sup>35</sup> In skin, which is also a collagen rich, multilayered tissue, the polarized reflectance signal distinguishes features of carcinomas, burn scars, and venous abnormalities.<sup>31,32</sup>

The primary purpose of this study is to assess the sensitivity of polarized reflectance microscopy to articular surface disruption of bovine cartilage explants. Because the polarized reflectance contrast parameter includes a reflectance signal derived from single scattering, multiple scattering, and birefringence,<sup>30</sup> it should be sensitive to both disruptions of the articular surface and damage to collagen microstructure in the superficial zone. To test this hypothesis, a polarization difference contrast parameter was calculated, and dependence on surface reflectance versus subsurface birefringence was assessed before and after several surface treatments of mechanical scrape, collagenase treatment, or both collagenase and scrape. The effects of explant treatments were assessed independently by surface marking with India ink, live/dead staining for chondrocyte viability, explant physical measurements, polarized light microscopy, and haematoxylin and eosin (H&E) staining of transverse histological sections. As part of this work, a Mueller matrix model of polarized reflectance from cartilage was developed to help explain trends in the experimental data. The findings demonstrate the feasibility of reflected polarized light microscopy in detecting microstructural alterations to the articular surface of cartilage explants. The technique is useful for biomechanical studies of cartilage explants requiring noninvasive surface and subsurface microstructural characterization without laser light irradiation of chondrocytes and cartilage extracellular matrix.

## 2 Materials and Methods

### 2.1 Explant Harvest

Adult bovine knees ( $N = 4$ ) were obtained fresh from a local abattoir within 24 h postmortem and kept on ice prior to harvest. The femur was clamped with a vise and soft tissues were removed to reveal the patellofemoral ridge. A 3-mm diameter dermal biopsy punch created cylindrical cartilage plugs still attached to the subchondral bone. Then, a surgical scalpel blade was used to undercut the cartilage plugs, creating 3-mm diameter cartilage explants. Explants were placed in microcentrifuge tubes containing phosphate-buffered saline (PBS) and kept on ice. Additional explants were taken from the weight-bearing region of the femoral condyles (FC). Experiments were performed immediately following the harvest.

### 2.2 Explant Treatment

The explant study was divided into two experiments (1 and 2). Experiment 1 compared the effects of differing surface treatments on polarized reflectance signals. Experiment 2 imaged explants following a progressive, controlled surface scrape, recording a polarized reflectance signal from explants treated with differing numbers of scrape passes. In experiment 1, explants were divided into three treatment groups: scrape, collagenase, and “both,” and one additional control “untreated” group ( $n = 10$  explants/group). In experiment 2, each group contained five explants and they were subjected to 1, 3, 5, 10, and 20 scrapes passes using sandpaper (see below). A subset of six explants from the FC were used to assess chondrocyte viability in scraped ( $n = 3$ ) versus untreated ( $n = 3$ ) explants. Chondrocyte viability was determined from fluorescence microscopy images following exposure to live/dead assay reagents (live/dead viability/cytotoxicity kit for mammalian cells, Thermo Fisher Scientific Inc., Massachusetts). Physical data of each explant, such as joint location, wet weight, and thickness, were collected before and after treatments. Explant height was measured by capturing a profile picture of an explant with a ruler to determine scale. The values were obtained by manual line-drawing in ImageJ (NIH Image, Bethesda, Maryland). The average of five equally spaced vertical lines from top to bottom of the explant was scaled by the ruler markings and defined as the explant height. Explant weight was measured by a mass balance (ML303T, Mettler-Toledo, Maryland). The details of the surface treatments are:

*Scrape group:* Scraping was performed by passing a piece of 600-grit ultrafine waterproof sandpaper with a 200-g weight on top across each explant traversing 5 cm (= 1 scrape). There were 10 scrapes performed on each explant in this group in experiment 1; in experiment 2, the numbers of scrapes varied from 1 to 20.

*Collagenase group:* Explants were incubated in enzyme solution contained 5 mg of collagenase type 1 (Sigma Aldrich, St. Louis, Missouri) dissolved in 20 ml solution of 0.36 nM  $\text{CaCl}_2$  and deionized water for 30 min at room temperature.

*“Both” group:* Explants were treated first with collagenase, and then with 10 scrape passes. Explants were rinsed with PBS in between treatments.

Following treatment, each explant was marked with India ink diluted to 25% in PBS by wiping a laboratory tissue dipped into India ink solution on the explant surface. The explants were rinsed with PBS to remove residual dye. India ink was used to reveals cracks and rough patches on the disrupted articular surface. One explant chosen from each group was kept ink-free for histology.

### 2.3 Reflectance Microscopy

Figure 1 shows the experimental setup, including explant harvest, treatments, and microscopy. An MT9300 polarized microscope (Meiji Techno Co., Ltd, Japan) with strain-free  $4\times/\text{N.A } 0.10$  and  $10\times/\text{N.A } 0.25$  objectives was used. An incident illuminator consisting of a halogen bulb with a transformer provided broad spectral bandwidth visible light that passed through a green transmission filter (546 nm wavelength) and polarizer to generate quasimonochromatic polarized light. The analyzer and polarizer were either in parallel (Par) or perpendicularly crossed (Per) positions, leading to bright or dark image backgrounds, respectively. Images were taken at those positions using a 5.0-megapixel CMOS camera (Lumenera Corp., Canada) mounted on the intermediate tube of the microscope and connected to the computer via a universal serial bus port. Explants were optically coupled to the glass coverslip by drops of PBS while the coverslip was placed at an angle to direct specular reflectance from the air-glass interface away from the light collection path. During the image acquisition, Par and Per images were collected serially and were coregistered. One field of view was recorded with microscope images from the central region of each explant and noted by aligning a razor nick in the cartilage with a corner of the image under a  $4\times$  objective. Then, the objective was switched to  $10\times$ . For repeated imaging, before versus after treatment, the alignment of the  $4\times$  image was checked to be the same. Other parameters, such as light intensity and exposure, were also kept the same.

### 2.4 Image Analysis

Images were acquired as  $1296 \times 968$  pixels images in .tif format by using camera software Infinity Capture (Lumenera Corp., Canada). Polarization contrast parameter maps were calculated from pairs of Per and Par images using the formula  $\text{Pol} = (\text{Par} - \text{Per}) / (\text{Par} + \text{Per})$ . The range of possible Pol image values was from 0 for equal signal in Per and Par pixels to a theoretical maximum of 1, corresponding to 0 signal in Per pixels. Negative Pol values were not found in this study, and typical Pol values ranged from 0.1 to 0.6. A value of 0 represents roughly equal contributions of signal from Par and Per configurations,

and minimal surface scattering, returned to the optical sensor at that image pixel. A value of 0.5 represents equal signal from the surface and deeper layers. Image processing and analysis was done using a custom-made MATLAB script. Data were presented as mean  $\pm$  SD (standard deviation). In Figs. 2–6 and 8, images were contrast-enhanced equally to bring out textural features.

### 2.5 Optical Model

To test the effects of alterations to tissue optical properties with surface treatments on polarized reflectance parameters, a simple model of polarized reflectance from tissue was adapted to articular cartilage by adding effects of superficial zone cartilage birefringence and depolarization at a roughened articular surface.<sup>31</sup> The original model by Jacques et al. represents the polarized reflectance signal intensity from tissue collected in the Par and Per configurations, with incident light intensity  $I_0$ . The signal intensities in these configurations are  $I_{\text{PAR}}$  and  $I_{\text{PER}}$ . Ignoring absorption, which is dominated by scattering in cartilage, the signal intensity depends upon superficially reflected ( $R_S$ ) and deeply penetrating back-scattered light ( $R_D$ ), to several scattering lengths, as

$$I_{\text{PAR}} = I_0(R_S + 0.5R_D), \quad (1)$$

$$I_{\text{PER}} = I_0(0.5R_D). \quad (2)$$

To apply Eqs. (1) and (2) to cartilage explants, the optical system is modeled using Mueller matrices, with each optical component represented as a  $4 \times 4$  matrix. The Mueller matrices representing horizontal and vertical polarizers are given by Refs. 36 and 37

$$M_{\text{LPH}} = \begin{bmatrix} 1 & 1 & 0 & 0 \\ 1 & 1 & 0 & 0 \\ 0 & 0 & 0 & 0 \\ 0 & 0 & 0 & 0 \end{bmatrix}. \quad (3)$$

$$M_{\text{LPV}} = \begin{bmatrix} 1 & -1 & 0 & 0 \\ -1 & 1 & 0 & 0 \\ 0 & 0 & 0 & 0 \\ 0 & 0 & 0 & 0 \end{bmatrix}. \quad (4)$$

The effect of collagen birefringence at the superficial layer acts as a linear retarder oriented at 45 deg ( $\theta = 45$  deg) to the polarization axes, with optical retardance  $\gamma$  in radians<sup>36,37</sup>

$$M_{\text{LR}} = \begin{bmatrix} 1 & 0 & 0 & 0 \\ 0 & \cos^2 2\theta + \cos \gamma \sin^2 2\theta & (1 - \cos \gamma) \sin 2\theta \cos 2\theta & \sin \gamma \sin 2\theta \\ 0 & (1 - \cos \gamma) \sin 2\theta \cos 2\theta & \sin^2 2\theta + \cos \gamma \cos^2 2\theta & -\sin \gamma \cos 2\theta \\ 0 & -\sin \gamma \sin 2\theta & \sin \gamma \cos 2\theta & \cos \gamma \end{bmatrix}. \quad (5)$$

The Mueller matrix representing the roughened articular surface is that of a diagonal depolarizer  $M_D$  with main diagonal elements of  $[1 \ M_{D(2,2)} \ M_{D(3,3)} \ M_{D(4,4)}]$ , where  $0 \leq M_{D(i,i)} \leq 1$  for  $i = 2, 3,$  and  $4,$  and 0 elsewhere.<sup>36</sup> In the absence of direct measurements of the depolarization matrix elements from cartilage, isotropic depolarization was chosen,

$M_{D(2,2)} = M_{D(3,3)} = M_{D(4,4)} = a,$  in part because this depolarization matrix is a component of others required to make them physically real, and in part because the optical system was not capable of measuring all nine nonzero elements of the generalized depolarization matrix.<sup>37</sup> Other depolarization Mueller matrices are possible<sup>37</sup> and the exact form of the depolarization

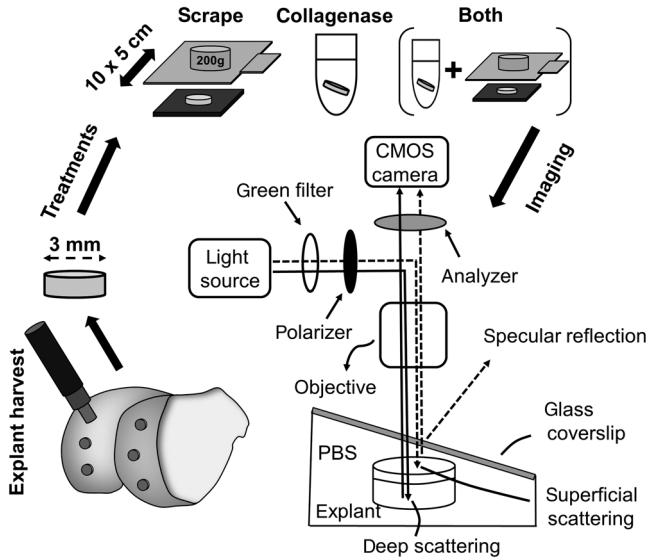


**Fig. 1** Schematic of the experimental task-flow and optical setup, including explant harvest, treatments, and microscopy. Explants were optically coupled to the glass coverslip by drops of PBS. The polarizer was fixed, while the analyzer axis was fully rotatable to be parallel (Par) and perpendicular (Per) to the axis of the polarizer.

matrix from articular cartilage is of significant interest for future study. In those cases, a comparison of model to experimental data would require a full Mueller matrix imaging polarimetry system. Several nonisotropic diagonal depolarization matrices were tested to confirm similarity of trends in the Pol parameter with the depolarization index,  $\Delta = 1 - |\text{tr}(M_D) - 1|/3$ ,<sup>38</sup>

$$M_D = \begin{bmatrix} 1 & 0 & 0 & 0 \\ 0 & a & 0 & 0 \\ 0 & 0 & a & 0 \\ 0 & 0 & 0 & a \end{bmatrix}. \quad (6)$$

For horizontal linear polarized incident light, the Stokes vector is  $S = [1 \ 1 \ 0 \ 0]^T$ . The fraction of total single scattering events from collagen  $x$  and a depolarization factor  $a$  both vary from 0 (low collagen scattering/high depolarization) to 1 (high collagen scattering/low depolarization). Equation (1) is split into three terms

$$I_{\text{PAR}} = I_0 [S_{\text{SURF,NC}}(0) + S_{\text{SURF,COL}}(0) + 0.5R_D]. \quad (7)$$

The first term  $S_{\text{SURF,NC}}(0) = M_{\text{LPH}}(1-a)(1-x)S$ , the first Stokes vector element representing total intensity, is superficial scattering, not from collagen ( $1-x$ ), modified by the Mueller matrix of the horizontal polarizer and the term  $(1-a)$  representing more scattering from a roughened surface. The element-wise matrix multiplication is scalar =  $(1 \times 4)(\text{scalar})(\text{scalar})(4 \times 1)$ . The second term is the first Stokes vector element representing total intensity of scattering from superficial subsurface collagen,  $S_{\text{SURF,COL}}(0) = M_{\text{LPH,row 1}}M_D, M_{\text{LR}}, M_D \times S$  affected by surface roughening (on tissue entrance and exit), collagen birefringence, and the horizontal polarizer. The element-wise matrix multiplication is scalar =  $(1 \times 4)(4 \times 4)(4 \times 4)(4 \times 4)(\text{scalar})(4 \times 1)$ . Equation (2) becomes

$$I_{\text{PER}} = I_0 [0.5R_D + S_{\text{SUBSURF,COL}}(0)], \quad (8)$$

where the second term  $S_{\text{SUBSURF,COL}}(0) = M_{\text{LPV}}M_DM_{\text{LR}}M_D \times S$ , is similarly derived from collagen birefringence modified by scattering losses at the cartilage surface. Finally, the Pol parameter is calculated as

$$\text{Pol} = (I_{\text{PAR}} - I_{\text{PER}})/(I_{\text{PAR}} + I_{\text{PER}}). \quad (9)$$

A surface plot of Pol intensity versus  $x$  and  $a$  was created using a custom-written MATLAB code.

## 2.6 Statistical Analysis

To determine the effect of explant treatments on explant physical characteristics, one-factor analysis of variance (ANOVA) was performed for change in explant wet weight and thickness. The relationship between the change in explant wet weight and thickness before and after treatments was assessed by linear correlation. To determine the effect of surface scrape on superficial chondrocytes and the articular surface, two-sample  $t$ -tests were performed for chondrocyte viability and India ink area fraction from untreated and scraped cartilage explants from the same region of bovine FC. To determine the effect of progressive scrape on the polarized reflectance signal, one-factor ANOVA was performed for the mean Pol value. To determine the effect of progressive scrape on articular surface damage and explant tissue loss, one-factor Kruskal–Wallis tests were performed for the India ink area fraction and change in explant wet weight, respectively. The relationship between the mean Pol value and India ink area fraction from the progressive scrape experiment was assessed by linear correlation analysis.

Before comparing posttreatment explant groups, variation was assessed in the Pol values pretreatment. The Pol values before treatment did not vary with group (Kruskal–Wallis test,  $p > 0.05$ ). All ANOVAs were performed after failing to reject assumptions of normality and homoscedasticity by Kolmogorov–Smirnov and Levene’s tests, respectively. Otherwise, the Kruskal–Wallis test was performed. Pairwise comparisons were performed following ANOVA to test differences between scrape, collagenase, and “both” treatments, and between 0, 1, 3, 5, 10, and 20 successive scrapes. Significance was set at  $p < 0.05$ .

## 3 Results

### 3.1 Polarized Reflectance from Scraped and Collagenase-Treated Explants

Representative polarized reflectance microscopy images from experiment 1 (Fig. 2) reveal reflectance features that vary over the four conditions: untreated, scraped, collagenase-treated, and “both” collagenase followed by scrape treatment. In all cases, Par images were brighter than Per images. The Pol parameter map, calculated from Par and Per images, reveals collagen in negative contrast, with lower Pol values and surface scattering features as higher Pol values. For untreated and collagenase-degraded explants, Pol parameter maps revealed a lattice-like texture of surface scattering and subsurface collagen birefringence features that were oriented at oblique angles in the Pol maps. Following mechanical scrape, image contrast worsened and the lattice texture was not distinguishable.

Pixel histograms from Pol parameter maps reveal characteristic shifts in the distributions of values within each field of view. For a scraped explant [Figs. 3(a)–3(d)], the Pol mean became higher, with positive-shifted kurtosis and negative-shifted skew

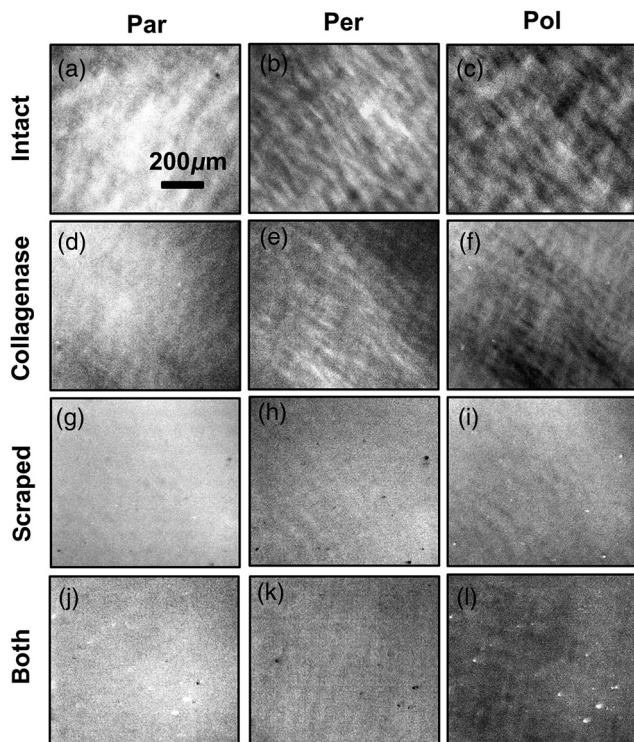


**Fig. 2** Representative 10 $\times$  images from Par (left column) and Per (middle column) configurations and calculated Pol parameter maps (right column) for (a)–(c) intact (untreated), (d)–(f) collagenase-treated, (g)–(i) mechanically scraped, and (j)–(l) both collagenase-treated and scraped explants. Scale is indicated.

compared to the Pol map from the same explant before treatment. Similarly, for a collagenase-treated explant [Figs. 3(e)–3(h)], the Pol mean became higher but with negative-shifted kurtosis and positive-shifted skew compared to the Pol map from the same explant before treatment.

Representative polarized reflectance microscopy Pol parameter images from experiment 2 reveal linear, striated reflectance features, similar to India-ink markings (Fig. 4). These striations appear in Pol images of explants treated with 1 to 5 scrape passes. Explants treated with 10 to 20 scrape passes had similar, low-contrast Pol images as scraped explants in experiment 1.

There were significant differences in mean Pol values, India ink area fraction, and change in explant wet weight between progressive scrape groups (Table 1). Specifically, Pol and India ink area fraction were higher with more scrape passes (1-factor ANOVA,  $p < 0.001$  for Pol; and 1-factor Kruskal–Wallis,  $p < 0.05$  for India ink area fraction). Explant wet weight was lower with more scrape passes (1-factor Kruskal–Wallis,  $p < 0.001$ ). Significant differences between scrape groups are indicated in Table 1. The mean Pol value following 5 to 20 scrapes was distinguishable from that of untreated and singly scraped explants. The India ink area fraction and change in explant wet weight were also different between all scrape groups and untreated explants. Significant pairwise comparisons are indicated in Table 1.

### 3.2 Transverse Section Histology and Birefringence Following Scrape and Enzymatic Treatments

Articular cartilage surface treatments altered the appearance of histology sections, both stained with H&E and unstained sections imaged with an orientation-independent birefringence

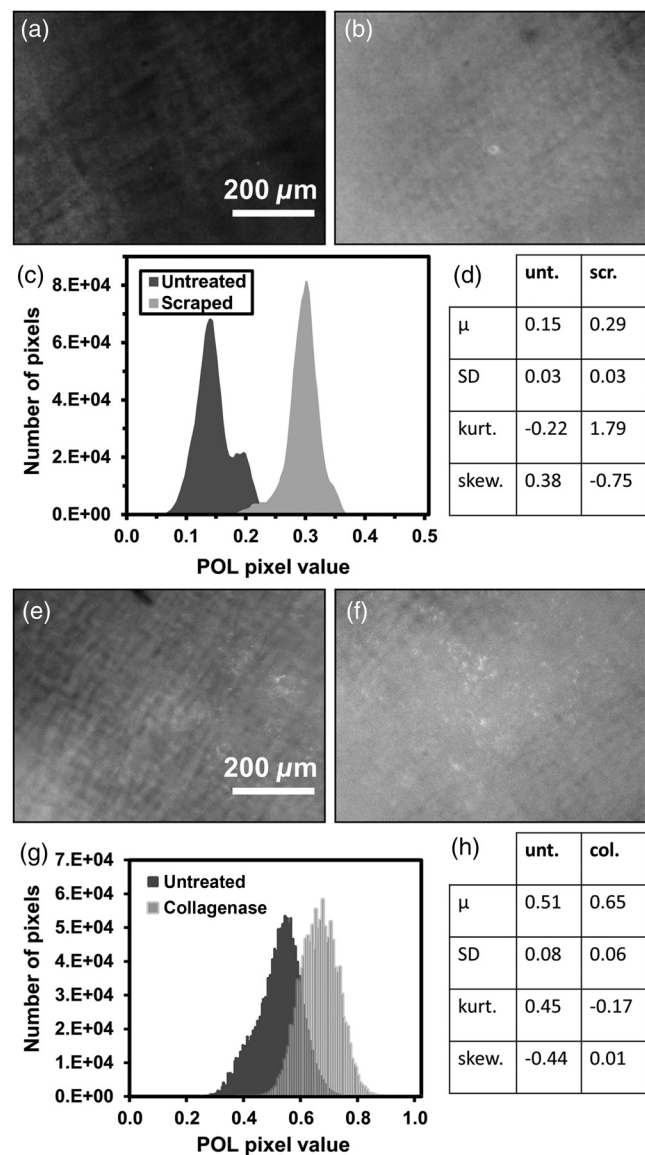


**Fig. 3** Alterations to Pol parameter maps and pixel histograms following scrape and collagenase treatments. From the same explant, Pol parameter maps (a) and (e) before and (b) after scraping and (f) collagenase treatment were used to generate (c) and (g) pixel histograms and (d) and (h) distribution statistics.  $\mu$ , mean; SD, standard deviation; kurt., kurtosis; and skew., skewness. Scale is indicated.

signal (Fig. 5). The sections from untreated explants had a smooth surface and intact, flattened chondrocyte lacunae [Fig. 5(a)]. A birefringence signal from the superficial zone of these explants was higher than the middle zone [Fig. 5(e)]. In collagenase-degraded explants, there was significantly less subsurface tissue staining, with larger chondrocyte lacunae [Fig. 5(b)]. The subsurface birefringence signal was much lower than in sections from untreated explants [Fig. 5(f)]. The surfaces of scrape-treated and “both” explants were roughened [Figs. 5(c) and 5(d)]. The birefringence signal from sections in scraped and “both” groups indicated a loss of the superficial zone [Figs. 5(g) and 5(h)].

In experiment 2, the effects of a single scrape were visible as a roughened articular surface in H&E-stained sections [Figs. 6(c) and 6(d)] versus untreated, Figs. 6(a) and 6(b). The roughened articular surface was also apparent following 3 and 5 successive

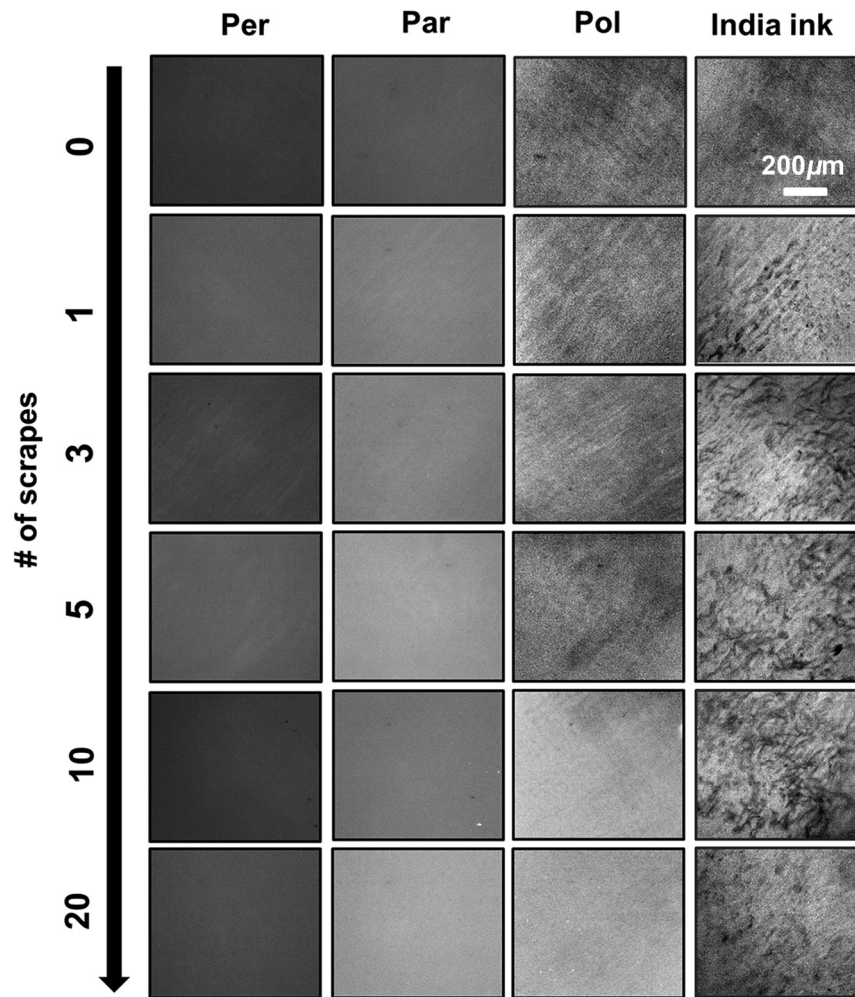


**Fig. 4** Representative images of Per (column 1) and Par (column 2) configurations, Pol maps (column 3) and images of India ink-stained cartilage explant surfaces (column 4), for untreated (first row, “0” label) explants and those treated with scrapes of increasing severity (numbers 1 to 20 in rows 2 to 6 correspond to the number of scrape passes). Scale bar is indicated.

**Table 1** Progressive scrape group parameters. For untreated (U-0) and scrape-treated (S-1 to S-20) explants, mean Pol parameter value, area fraction of India ink, and change in wet weight from before to after treatment were tabulated. Numbers are group mean  $\pm$  SD for  $n = 5$  to 6 explants/group. Superscript letters indicate the significance of *post hoc* pairwise comparisons.

Scr./Unscr.-# scr	Mean Pol	India ink area fraction (%)	$\Delta$ wet weight (mg)
U-0	0.15 $\pm$ 0.03	1.1 $\pm$ 1.1	0.0 $\pm$ 0.1
S-1	0.19 $\pm$ 0.06	5.4 $\pm$ 6.4 <sup>a</sup>	-0.7 $\pm$ 0.3 <sup>a</sup>
S-3	0.25 $\pm$ 0.06	7.9 $\pm$ 5.8 <sup>a</sup>	-1.1 $\pm$ 0.3 <sup>a,b</sup>
S-5	0.31 $\pm$ 0.06 <sup>a,b</sup>	4.4 $\pm$ 1.5 <sup>a</sup>	-1.2 $\pm$ 0.2 <sup>a,b</sup>
S-10	0.32 $\pm$ 0.04 <sup>a,b</sup>	8.7 $\pm$ 5.8 <sup>a</sup>	-1.0 $\pm$ 0.2 <sup>a</sup>
S-20	0.30 $\pm$ 0.05 <sup>a,b</sup>	4.5 $\pm$ 1.3 <sup>a</sup>	-2.0 $\pm$ 0.6 <sup>a,b,c,d,e</sup>

<sup>a</sup>U-0,  
<sup>b</sup>S-1,  
<sup>c</sup>S-3,  
<sup>d</sup>S-5, and  
<sup>e</sup>S-10.

scrapes [Figs. 6(e)–6(h)], but the articular surface became smoother after 10 and 20 scrapes [Figs. 6(i)–6(l)]. Orientation-independent birefringence also revealed a superficial zone of high birefringence that was visible in explants treated with 0 to 10 successive scrapes [Figs. 6(b), 6(d), 6(f), 6(h), 6(j)], but absent from explants treated with 20 successive scrapes [Fig. 6(l)].

### 3.3 Alteration of Explant Physical Properties by the Surface Treatments

Figure 7 shows the change in physical characteristics, wet weight, and thickness of each explant group before versus after the treatments. Explants in control and collagenase groups experienced no significant alterations in wet weight and thickness. The changes in wet weight were measured as  $\Delta$ ww = 0.06  $\pm$  0.34 mg for untreated and 0.29  $\pm$  0.95 mg for collagenase ( $n = 10$  explants per group). The changes in thickness were captured as  $\Delta$ h = 0.02  $\pm$  0.10 mm for control and 0.02  $\pm$  0.13 mm for collagenase-treated explants. In contrast, mechanical scraping and “both” scrape + collagenase groups showed a significant decrease in weight and height [ $\Delta$ ww = -1.41  $\pm$  0.67 mg,  $\Delta$ h = -0.29  $\pm$  0.13 mm in scrape;  $\Delta$ ww = -1.27  $\pm$  0.77 mg,

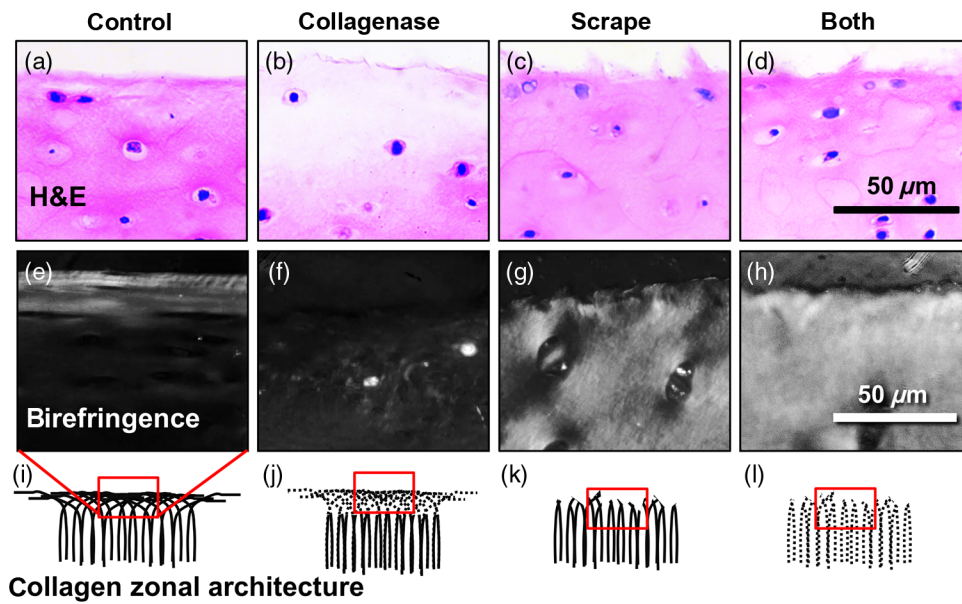


**Fig. 5** Surface treatment altered the histological appearance of articular cartilage explants. (a)–(d) H&E staining and (e)–(h) orientation-independent birefringence from (a) and (e) untreated control, (b) and (f) collagenase-treated, (c) and (g) scrape-treated, and (d)–(h) collagenase plus scrape-treated explants. (i)–(l) Collagen network zonal architecture corresponding to the histology images are depicted within the red region of interest. Solid lines are intact collagen fibrils; dashed lines are collagenase-degraded collagen fibrils. Scale is indicated.

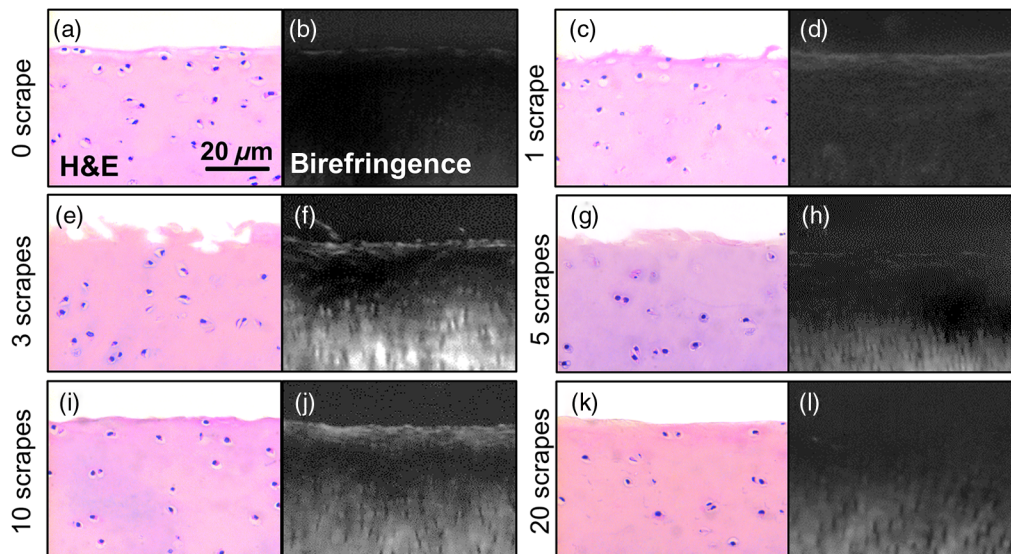


**Fig. 6** Histological appearance of explants following progressive scrapes of (a) and (b) 0, (c) and (d) 1, (e) and (f) 3, (g) and (h) 5, (i) and (j) 10, and (k) and (l) 20 passes, by (a), (c), (e), (g), (i), (k) H&E, and (b), (d), (f), (h), (j), (l) orientation-independent birefringence. Scale bar is indicated.

$\Delta h = -0.25 \pm 0.12$  mm in “both,” Figs. 5(a) and 5(b)]. The change in wet weight and thickness of individual explants was positively correlated [Fig. 7(c),  $R^2 = 0.65$ ].

### 3.4 Superficial Chondrocyte Viability and India Ink Marking with Surface Scrape

Superficial chondrocyte viability in femoral condyle explants obtained from LIVE/DEAD<sup>®</sup> assay (Molecular Probes, Eugene, Oregon) fluorescent images [Figs. 8(a), 8(b), 8(e), 8(f)] showed a higher number of dead cells and fewer live cells in the scrape-

treated group than in the untreated ones. Note that quantification of cell viability was  $71\% \pm 1\%$  prior to scrape and reduced to  $40\% \pm 2\%$  after scrape [Fig. 8(i),  $p < 0.001$  by Student’s  $t$ -test]. Likewise, the Pol maps of intact explants displayed a lattice texture [Fig. 8(c)] with retained India ink in small and sparse stipple patterns [Fig. 8(d)]. The scraped explants revealed loss of texture from birefringence features [Fig. 8(g)] along with more ink in striated marks on the surface [Fig. 8(h)]. The India ink area fraction was higher following scrape ( $7.5\% \pm 2.3\%$  in untreated versus  $48\% \pm 2.3\%$  in scrape-treated explants, Fig. 6(j),  $p < 0.001$  by Student’s  $t$ -test).

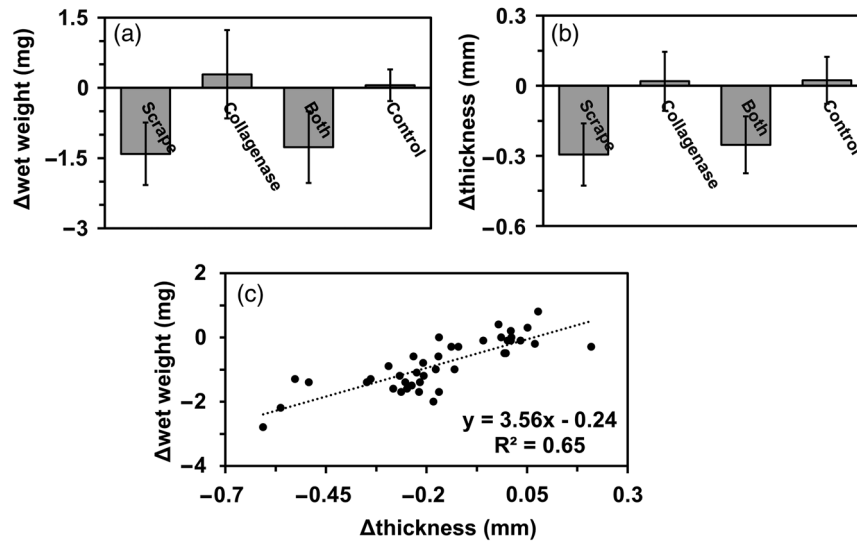


**Fig. 7** Explant physical alterations after treatment. Change in (a) wet weight, (b) thickness, and (c) the correlation between wet weight and thickness of adult bovine cartilage explants ( $n = 40$ ), treated as indicated.

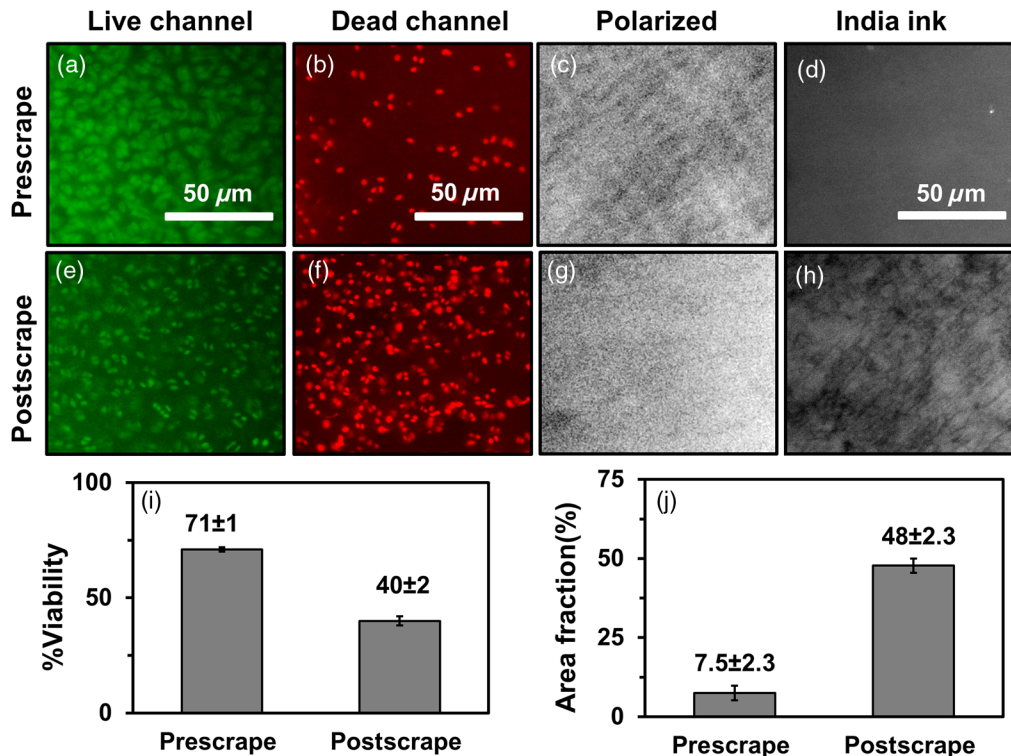


**Fig. 8** The effects of mechanical scrape on chondrocyte viability. Images of cartilage explants (a)–(d) before and (e)–(h) after scrape treatment. Representative epifluorescence images of live/dead stained articular surfaces in the [green, (a), (e)] live and [red, (b), (f)] dead channels. Representative (c) and (g) Pol parameter maps and (d) and (h) reflectance images of India ink-marked articular surfaces. Scale bars are indicated. The average (i) chondrocyte viability and (j) India ink area fraction pre- versus postscrape.

### 3.5 Sensitivity of Polarized Reflectance Signal to Progressive Mild Surface Scrape

The sensitivity of the Pol parameter to surface scraping of adult bovine knee articular cartilage explants was assessed by correlation of Pol with India ink area fraction (Fig. 9). The mean Pol parameter correlated significantly and positively with India ink area fraction, stronger for explants with India ink covering <8%

of the image area ( $R^2 = 0.42$ , Fig. 9, blue circle). The correlation was lower when explants with higher India ink area fractions were included ( $R^2 = 0.20$ , Fig. 9, red circle).

### 3.6 Optical Model of Polarized Reflectance Contrast Parameter

The optical model produced Pol values as a function of the fraction of total scattering from collagen  $x$  and the depolarization

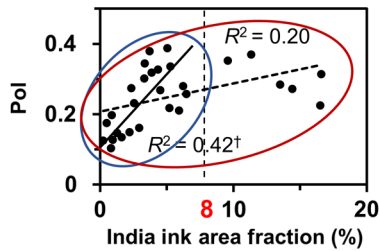


**Fig. 9** A correlation plot of the mean Pol parameter and India ink area fraction from cartilage explants following 1 to 20 scrape passes (6 groups, 5 samples/group).  $p < 0.05$ ,  $\dagger p < 0.01$ .

parameter  $a$  (Fig. 10). The Pol value varied from 0 to 0.8 and was highest for small values of  $x$  and  $a$  [Fig. 10(a)]. Higher Pol values occur with lower  $x$  at fixed  $a = 0.25$  and with lower  $a$  at fixed  $x = 0.25$  [Fig. 10(b)].

The deep reflection coefficient  $R_D$  was assigned a value of 0.35, based on a reasonable assumption that the scattered intensity  $e^{-2\mu x}$  drops to 35% at half a scattering length. The trend of higher Pol with less collagen scattering and more depolarization was insensitive to variation in  $R_D$  from 0 to 1, or to anisotropic depolarization, where  $M_{D,\text{trace}} = [1 \ a \ b \ c]$  and in general  $0 \leq a \neq b \neq c \leq 1$ . Although the trends were invariant, the absolute values of the Pol parameter were influenced by altering  $R_D$  and  $M_D$ , for a given amount of collagen scattering and total depolarization (data not shown).

#### 4 Discussion

The polarized reflectance signal from bovine articular cartilage is sensitive to treatments that alter the microscale topography at the articular surface and subsurface collagen. Particularly, abrasive scrape resulted in a higher mean Pol parameter [Fig. 3(c) and Table 1]. Correspondingly, mild scrapes produced linear reflectance features that corresponded to India ink markings (Fig. 4) and an uneven surface of histological sections (Fig. 6). More extensive scraping led to loss of surface and subsurface reflectance features, lower explant wet weight, lower explant thickness (Table 1), and death of chondrocytes within the superficial zone (Fig. 8). Brief collagenase treatment lowered the birefringence signal under crossed polarizers [Figs. 3(e)–3(g)] and altered the appearance of the superficial zone in histological

sections [Fig. 5(f)]. A model incorporating the effects of collagen birefringence and signal depolarization at the articular surface confirmed a trend of higher Pol values with less scattering from collagen and/or more depolarization at the articular surface [Fig. (10)]. Depolarization caused by surface scattering and/or loss of superficial collagen may also explain the loss of sensitivity of Pol to India ink area fractions  $>8\%$  (Fig. 9). Together, these data suggest that polarized reflectance microscopy is an effective tool to noninvasively assess alterations to cartilage explant surfaces and superficial subsurface tissue.

The polarization reflectance signal is influenced by light scattering in cartilage, as well as by birefringence from collagen fibrils. In the explants studies here, normal scattering is altered mainly by surface roughening with sandpaper. Birefringence depends on the thickness, collagen content, and organization of the collagen network in the superficial zone.<sup>19,26,34</sup> In previous studies, the anisotropy and orientation of the collagen network from cervical tissue has also been mapped quantitatively using OCT<sup>39</sup> and polarimetric colposcopy.<sup>40</sup> Significantly, polarimetric imaging distinguishes between healthy cervical tissue, revealing subepithelial collagen birefringence, and dysplastic lesions, which have lower depolarization values, potentially due to remodeling or degradation of the collagen network.<sup>41</sup> In the untreated explants, the birefringence signal in the Per channel is consistent with the orientation and anisotropy of the tangentially aligned collagen network in the superficial zone.<sup>33</sup> *En face* superficial collagen network orientation in bovine cartilage varied less over several mm than in chick articular cartilage, based on comparing the birefringence orientation-dependence from the bovine explants with measurements made from a second harmonic generation signal in chick cartilage.<sup>39</sup> This allowed the accurate measurement of the Pol parameter by rotating the explant to capture the maximum birefringence, with collagen alignment at 45 deg to both the polarizer and analyzer directions. Superficial collagen alignment is also revealed by a “brushing direction” in bovine articular cartilage, observed with polarization-sensitive OCT using a conical scanning technique.<sup>40</sup> Conical-scanning OCT specifies the superficial collagen fiber alignment over a full 360 deg, whereas linear birefringence detection techniques only specify alignment over 180 deg. However, the combination of information provided by birefringence and surface reflectance measurements in the Per and Par channels, respectively, using the current technique, provides

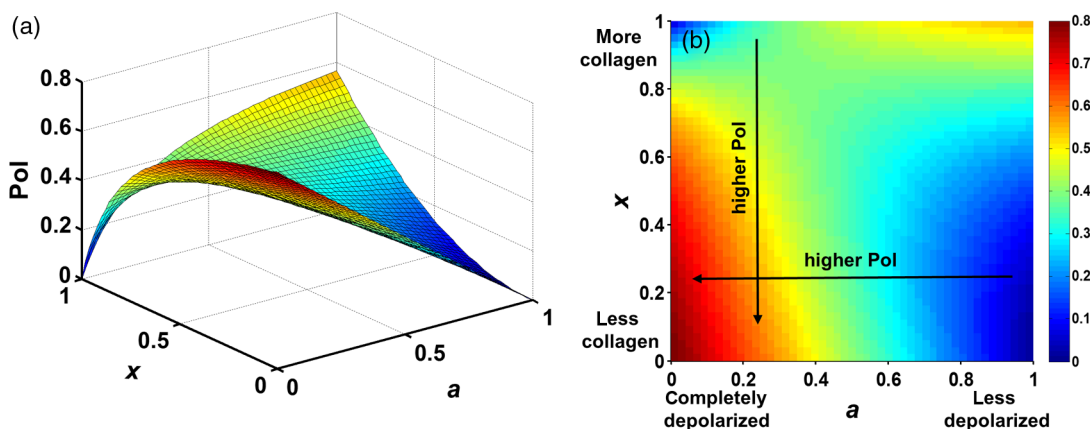


**Fig. 10** (a) A 3-D surface map and (b) two-dimensional parametric colormap of Pol values versus total scattering from collagen  $x$  and the depolarization parameter  $a$  based on the mathematical model. Trends of higher Pol values at fixed  $x$  and  $a$  are indicated by the black arrows.

useful and complementary information usually accessible only through histological sectioning.

The Pol parameter decouples surface roughening from the loss of superficial collagen and identifies several distinct alterations. Mild surface roughening without the loss of superficial collagen produces a Pol parameter map with scrape and collagen in positive and negative contrast, respectively (Fig. 4, 1–3 scrapes). Extensive surface roughening and/or erosion of the superficial zone lowers Pol map texture and contrast [Figs. 2(i), 3(b), 8(g)]. The alteration in polarimetric contrast with progressive scrape was most prominent after 10 and 20 scrapes (Fig. 4). The explants scraped 10 times had the highest India ink area fraction, 8.7%, while losing 1 mg wet weight. Explants scraped 20 times had the largest loss of wet weight, at 2 mg but less ink-retaining surface features, at 4.5% (Table 1). These data point to two possible reasons for the loss of polarimetric contrast: more depolarization from surface scattering with retention of superficial zone collagen birefringence after 10 scrapes [Fig. 6(j)], or removal of superficial zone tissue with the loss of collagen birefringence after 20 scrapes [Fig. 6(l)]. Depolarization caused by surface scattering also may explain the loss of sensitivity of Pol to India ink area fractions  $>8\%$  (Fig. 9). Preservation of the articular surface with enzymatic degradation of collagen leads to a higher mean Pol with reduced collagen contrast [Figs. 2(f), 3(f)]. The optical model clarifies reasons for the loss of polarized reflectance texture and alterations in the Pol average [Fig. 10(b)]. The birefringence signal is lowered when collagen is degraded or removed, encoded by the fraction of collagen scatterers  $x$  and is obscured and depolarized by diffuse surface scattering, encoded by the depolarization factor  $a$ . Comparison of experimental data to model trends suggested that the loss of polarimetric contrast occurred following scrape-removal of aligned collagen, assessed by the loss of explant wet weight (Table 1) and superficial birefringence from transverse sections (Fig. 6), and depolarization of the birefringence signal by surface scattering, assessed by India ink features and image area fraction (Figs. 4, 9, Table 1). To further explain the absolute sensitivity of Pol to cartilage birefringence and depolarization would require measurements of  $R_D$  and  $M_D$  as inputs to the model of Fig. 10. Therefore, alterations to the cartilage articular surface and superficial zone are sensitively detected by polarized reflectance microscopy.

Variation in Pol values within explants is expected due to variability in collagen zonal architecture, articular surface topography, and swelling properties of the cartilage. To reduce this variation, all images were recorded in a central region that was tracked using a 4 $\times$  objective with wider field of view, encompassing the explant edges. This region was flattest, assessed by scanning the objective focus across the explant surface, and least likely to suffer from edge effects (e.g., cartilage swelling). In future studies, the Pol map may be extended spatially by stitching together Par and Per images from overlapping fields of view. The coefficient of the variation of mean Pol from eight fields of view within a 5  $\times$  5 mm<sup>2</sup> region of the articular surface was measured to be 0.11, indicating the level of variation expected from normal adult bovine articular cartilage.

In comparison to more advanced laser-based techniques to image cartilage microstructure, polarized reflectance microscopy has several strengths and weaknesses. The polarized reflectance technique is simple, provides rapid image acquisition with wide surface coverage, and a quantitative parameter map (the Pol parameter) calculated from just two images.<sup>31</sup> The

Pol parameter includes information from surface and superficial subsurface tissue probed by the illumination source. The axial resolution of polarized reflectance microscopy is not as great as conventional confocal and two-photon microscopy, which is  $\sim 0.5 \mu\text{m}$  at best.<sup>41,42</sup> In contrast, nondepth resolved reflectance microscopy recovers information from  $\sim 300\text{-}\mu\text{m}$  depth in scattering tissue in a single frame.<sup>31</sup> However, polarized reflectance effectively and rapidly probes the superficial zone of bovine articular cartilage, which is usually  $<300\text{-}\mu\text{m}$  thick.<sup>43–45</sup> Separation of the polarized reflectance into Par and Per channels effectively selects for predominantly single, superficial scattering, and birefringent, subsurface scattering, respectively. Therefore, the reflectance signals that generate the Pol parameter map are poised to respond sensitively to alterations of the articular surface and subsurface, an area of active remodeling in biomechanical and mechanobiological studies of cartilage explants.

Optical assessment by polarized reflectance microscopy may benefit cartilage explant studies of traumatic injury, growth, maturation, and degeneration. Injurious mechanical loads applied to cartilage explants produce surface cracks and tissue deformation.<sup>9,10</sup> It would be interesting to study alterations to surface birefringence following severe mechanical loading. Immature cartilage possesses lower levels of collagen<sup>46</sup> than mature cartilage<sup>6</sup> and lacks a mature zonal architecture.<sup>47,48</sup> Explant studies of *in vitro* growth and maturation of immature cartilage could benefit from polarized reflectance microscopy, which could be performed nondestructively and repetitively on the same individual explants before, during, and after treatment with growth factors. Similarly, the superficial microstructure of explants undergoing degeneration *in vitro* following exposure to catabolic factors, such as IL-1 $\beta$  and TNF- $\alpha$ , could be tracked during cartilage degeneration and recovery. Other optical techniques such as confocal microscopy exist for noninvasive assessment of cartilage microstructure using laser-induced reflectance signals. The expense of confocal microscopy and difficulty in regulating phototoxicity resulting from laser irradiation<sup>49</sup> make polarized reflectance microscopy a reasonable alternative when repetitive optical measurements from explants are required.

Several developments and future experiments would enhance the translational relevance of polarized reflectance microscopy, as well as its usefulness for cartilage explant studies. For translational relevance, polarized reflectance microscopy could be performed on intact human cartilage fragments from donors or discarded postarthroplasty. A careful comparison of reflectance features and Pol parameter values with standard cartilage histopathology scores from colocalized transverse sections, such as the International Cartilage Repair Society (ICRS) or Osteoarthritis Research Society International scores, would test quantitative reflectance signal sensitivity versus established semiquantitative assessments.<sup>50–52</sup> Combining polarized reflectance in the visible wavelengths with polarized reflectance and absorbance in the infrared could yield noninvasive assessment of collagen, proteoglycan, and water content of superficial cartilage,<sup>53–55</sup> colocalized with surface and birefringence microstructural features. Polarized infrared microscopy has already been explored in transverse cartilage sections and suggested for use in the reflectance configuration.<sup>56</sup> The combination of microstructural and biochemical information from visible polarized reflectance and infrared remittance would yield more useful information on the status of the articular surface and subsurface. Finally, Monte Carlo simulation of polarized reflectance from a multilayered tissue<sup>57–59</sup> would help to clarify the trends described

by the simple optical model and experimental data presented in this study.

In conclusion, polarized reflectance microscopy is a useful noninvasive optical technique to assess microstructural alterations to the articular surface of cartilage explants. Reflected polarized optical signals derived from cartilage depend on surface scattering, subsurface multiple scattering, and linear birefringence.<sup>30,31</sup> Light penetration into articular cartilage effectively probes the superficial zone as well as the optical properties of the articular surface. The simple implementation and quantitative nature of polarized reflectance microscopy warrants further development for biomechanical and microstructural studies of articular cartilage. The utility of this optical technique for assessment of articular cartilage could be enhanced by incorporating multiwavelength acquisition, including in the infrared.

### Disclosures

The authors declared no conflicts of interest.

### Acknowledgments

We would like to thank Cristina Butrico for assistance with initial image processing and pilot experiments. Financial assistance from the School of Engineering at The Catholic University of America (New Millennium Fellowship, RH) is acknowledged. Financial support from the School of Engineering's Burns Fellowship (CBR) is acknowledged.

### References

- J. Katta et al., "Biotribology of articular cartilage—a review of the recent advances," *Med. Eng. Phys.* **30**(10), 1349–1363 (2008).
- R. M. Schinagl et al., "Video microscopy to quantitate the inhomogeneous equilibrium strain within articular cartilage during confined compression," *Ann. Biomed. Eng.* **24**(4), 500–512 (1996).
- M. F. Venn, "Chemical composition of human femoral and head cartilage: influence of topographical position and fibrillation," *Ann. Rheum. Dis.* **38**(1), 57–62 (1979).
- A. Maroudas, "Physicochemical properties of cartilage in the light of ion exchange theory," *Biophys. J.* **8**(5), 575–595 (1968).
- A. Maroudas, H. Muir, and J. Wingham, "The correlation of fixed negative charge with glycosaminoglycan content of human articular cartilage," *Biochim. Biophys. Acta* **177**(3), 492–500 (1969).
- M. M. Temple-Wong et al., "Biomechanical, structural, and biochemical indices of degenerative and osteoarthritic deterioration of adult human articular cartilage of the femoral condyle," *Osteoarthritis Cartilage* **17**(11), 1469–1476 (2009).
- J. C. Y. Hu and K. A. Athanasiou, "The role of mechanical forces in tissue engineering of articular cartilage," in *Functional Tissue Engineering*, F. Guilak, D. L. Butler, S. A. Goldstein, and D. J. Mooney, Eds., pp. 227–242, Springer, New York (2003).
- M. M. Temple et al., "Age- and site-associated biomechanical weakening of human articular cartilage of the femoral condyle," *Osteoarthritis Cartilage* **15**(9), 1042–1052 (2007).
- V. Morel and T. M. Quinn, "Short-term changes in cell and matrix damage following mechanical injury of articular cartilage explants and modelling of microphysical mediators," *Biorheology* **41**(3–4), 509–519 (2004).
- T. M. Quinn et al., "Matrix and cell injury due to sub-impact loading of adult bovine articular cartilage explants: effects of strain rate and peak stress," *J. Orthop. Res.* **19**(2), 242–249 (2001).
- A. Asanbaeva et al., "Mechanisms of cartilage growth: modulation of balance between proteoglycan and collagen in vitro using chondroitinase ABC," *Arthritis Rheum.* **56**(1), 188–198 (2007).
- N. T. Balcom et al., "In vitro articular cartilage growth with sequential application of IGF-1 and TGF-beta1 enhances volumetric growth and maintains compressive properties," *J. Biomech. Eng.* **134**(3), 031001 (2012).
- A. Asanbaeva et al., "Regulation of immature cartilage growth by IGF-I, TGF-beta1, BMP-7, and PDGF-AB: role of metabolic balance between fixed charge and collagen network," *Biomech. Model. Mechanobiol.* **7**(4), 263–276 (2008).
- J. Kinnunen et al., "Optical spectral imaging of degeneration of articular cartilage," *J. Biomed. Opt.* **15**(4), 046024 (2010).
- M. M. Temple et al., "Interleukin-1alpha induction of tensile weakening associated with collagen degradation in bovine articular cartilage," *Arthritis Rheum.* **54**(10), 3267–3276 (2006).
- N. Fukui et al., "Stimulation of BMP-2 expression by pro-inflammatory cytokines IL-1 and TNF-alpha in normal and osteoarthritic chondrocytes," *J. Bone Jt. Surg.* **85**(Suppl 3), 59–66 (2003).
- D. M. Bear et al., "Optical coherence tomography detection of sub-clinical traumatic cartilage injury," *J. Orthop. Trauma.* **24**(9), 577–582 (2010).
- J. Kinnunen et al., "Nondestructive fluorescence-based quantification of threose-induced collagen cross-linking in bovine articular cartilage," *J. Biomed. Opt.* **17**(9), 0970031 (2012).
- A. T. Yeh et al., "Nonlinear optical microscopy of articular cartilage," *Osteoarthritis Cartilage* **13**(4), 345–352 (2005).
- G. Meachim, "Light microscopy of Indian ink preparations of fibrillated cartilage," *Ann. Rheum. Dis.* **31**(6), 457–464 (1972).
- C. R. Chu et al., "Clinical diagnosis of potentially treatable early articular cartilage degeneration using optical coherence tomography," *J. Biomed. Opt.* **12**(5), 051703 (2007).
- J. M. Herrmann et al., "High resolution imaging of normal and osteoarthritic cartilage with optical coherence tomography," *J. Rheumatol.* **26**(3), 627–635 (1999).
- X. Li et al., "High-resolution optical coherence tomographic imaging of osteoarthritic cartilage during open knee surgery," *Arthritis Res. Ther.* **7**(2), R318–323 (2005).
- J. S. Bell et al., "Micromechanical response of articular cartilage to tensile load measured using nonlinear microscopy," *Acta Biomater.* **10**(6), 2574–2581 (2014).
- T. Xie et al., "Topographical variations in the polarization sensitivity of articular cartilage as determined by polarization-sensitive optical coherence tomography and polarized light microscopy," *J. Biomed. Opt.* **13**(5), 054034 (2008).
- B. J. Wong et al., "Two-photon excitation laser scanning microscopy of human, porcine, and rabbit nasal septal cartilage," *Tissue Eng.* **7**(5), 599–606 (2001).
- J. C. Mansfield et al., "Collagen fiber arrangement in normal and diseased cartilage studied by polarization sensitive nonlinear microscopy," *J. Biomed. Opt.* **13**(4), 044020 (2008).
- K. Kocsis et al., "Combination of digital image analysis and polarization microscopy: theoretical considerations and experimental data," *Microsc. Res. Technol.* **43**(6), 511–517 (1998).
- J. Rieppo et al., "Practical considerations in the use of polarized light microscopy in the analysis of the collagen network in articular cartilage," *Microsc. Res. Technol.* **71**(4), 279–287 (2008).
- S. L. Jacques, S. Roussel, and R. Samatham, "Polarized light imaging specifies the anisotropy of light scattering in the superficial layer of a tissue," *J. Biomed. Opt.* **21**(7), 071115 (2016).
- S. L. Jacques, J. C. Ramella-Roman, and K. Lee, "Imaging skin pathology with polarized light," *J. Biomed. Opt.* **7**(3), 329–340 (2002).
- S. L. Jacques, J. R. Roman, and K. Lee, "Imaging superficial tissues with polarized light," *Lasers Surg. Med.* **26**(2), 119–129 (2000).
- A. Benninghoff, "Der Aufbau des Gelenkknorpels in seinen Beziehungen zur Funktion. Zeitschrift für Zellforschung und mikroskopische," *Z. Zellforsch. Mikroskop. Anat.* **2**, 783–862 (1925).
- Y. E. Yarker, R. M. Aspden, and D. W. Hukins, "Birefringence of articular cartilage and the distribution on collagen fibril orientations," *Connect. Tissue Res.* **11**(2–3), 207–213 (1983).
- N. Ghosh et al., "Mueller matrix decomposition for polarized light assessment of biological tissues," *J. Biophotonics* **2**(3), 145–156 (2009).
- O. Svensen et al., "Mueller matrix measurements and modeling pertaining to Spectralon white reflectance standards," *Opt. Express* **20**(14), 15045–15053 (2012).
- H. D. Noble, S. C. McClain, and R. A. Chipman, "Mueller matrix roots depolarization parameters," *Appl. Opt.* **51**(6), 735–744 (2012).
- N. Ghosh, M. F. Wood, and I. A. Vitkin, "Mueller matrix decomposition for extraction of individual polarization parameters from complex turbid

- media exhibiting multiple scattering, optical activity, and linear birefringence," *J. Biomed. Opt.* **13**(4), 044036 (2008).
39. P. G. Ellingsen et al., "Quantitative characterization of articular cartilage using Mueller matrix imaging and multiphoton microscopy," *J. Biomed. Opt.* **16**(11), 116002 (2011).
  40. Z. Lu, D. Kasaragod, and S. J. Matcher, "Conical scan polarization-sensitive optical coherence tomography," *Biomed. Opt. Express* **5**(3), 752–762 (2014).
  41. B. Bailey et al., "Enhancement of axial resolution in fluorescence microscopy by standing-wave excitation," *Nature* **366**(6450), 44–48 (1993).
  42. W. R. Zipfel, R. M. Williams, and W. W. Webb, "Nonlinear magic: multiphoton microscopy in the biosciences," *Nat. Biotechnol.* **21**(11), 1369–1377 (2003).
  43. A. K. Jeffery et al., "Three-dimensional collagen architecture in bovine articular cartilage," *J. Bone Joint Surg. Br.* **73**(5), 795–801 (1991).
  44. J. P. Wu, T. B. Kirk, and M. H. Zheng, "Study of the collagen structure in the superficial zone and physiological state of articular cartilage using a 3D confocal imaging technique," *J. Orthop. Surg. Res.* **3**, 29 (2008).
  45. J. D. Rubenstein et al., "Effects of collagen orientation on MR imaging characteristics of bovine articular cartilage," *Radiology* **188**(1), 219–226 (1993).
  46. T. J. Klein et al., "Depth-dependent biomechanical and biochemical properties of fetal, newborn, and tissue-engineered articular cartilage," *J. Biomech.* **40**(1), 182–190 (2007).
  47. P. Julkunen et al., "Biomechanical, biochemical and structural correlations in immature and mature rabbit articular cartilage," *Osteoarthritis Cartilage* **17**(12), 1628–1638 (2009).
  48. M. C. van Turnhout et al., "Postnatal development of collagen structure in ovine articular cartilage," *BMC Dev. Biol.* **10**, 62 (2010).
  49. M. D. Cahalan et al., "Two-photon tissue imaging: seeing the immune system in a fresh light," *Nat. Rev. Immunol.* **2**(11), 872–880 (2002).
  50. P. Mainil-Varlet et al., "A new histology scoring system for the assessment of the quality of human cartilage repair: ICRS II," *Am. J. Sports Med.* **38**(5), 880–890 (2010).
  51. M. Rutgers et al., "Evaluation of histological scoring systems for tissue-engineered, repaired and osteoarthritic cartilage," *Osteoarthritis Cartilage* **18**(1), 12–23 (2010).
  52. K. P. Pritzker et al., "Osteoarthritis cartilage histopathology: grading and staging," *Osteoarthritis Cartilage* **14**(1), 13–29 (2006).
  53. I. O. Afara et al., "Spatial mapping of proteoglycan content in articular cartilage using near-infrared (NIR) spectroscopy," *Biomed. Opt. Express* **6**(1), 144–154 (2015).
  54. C. M. McGoverin et al., "The contribution of bone and cartilage to the near-infrared spectrum of osteochondral tissue," *Appl. Spectrosc.* **68**(10), 1168–1175 (2014).
  55. M. V. Padalkar, R. G. Spencer, and N. Pleshko, "Near infrared spectroscopic evaluation of water in hyaline cartilage," *Ann. Biomed. Eng.* **41**(11), 2426–2436 (2013).
  56. N. Ramakrishnan, Y. Xia, and A. Bidthanapally, "Polarized IR microscopic imaging of articular cartilage," *Phys. Med. Biol.* **52**(15), 4601–4614 (2007).
  57. M. Sun et al., "Characterizing the microstructures of biological tissues using Mueller matrix and transformed polarization parameters," *Biomed. Opt. Express* **5**(12), 4223–4234 (2014).
  58. J. C. Ramella-Roman, S. A. Prah, and S. L. Jacques, "Three Monte Carlo programs of polarized light transport into scattering media: part II," *Opt. Express* **13**(25), 10392–10405 (2005).
  59. J. Ramella-Roman, S. Prah, and S. Jacques, "Three Monte Carlo programs of polarized light transport into scattering media: part I," *Opt. Express* **13**(12), 4420–4438 (2005).

**Ruby N. Huynh** received her BS degree in biomedical engineering from The Catholic University of America (CUA). She is a graduate student researcher in the Department of Biomedical Engineering at CUA, under supervision of Dr. Chris Raub. She is currently working on techniques for quantitative microscopy and modeling of optical reflectance signals from articular cartilage.

**George Nehmetallah** is an assistant professor in the EECS Department at CUA. His research interests are in 3-D imaging and digital holography. He has served as a PI for several SBIR and STTR projects from Air Force, Army, NASA, and DARPA. He has authored a book on analog and digital holography with MATLAB and published more than 90 refereed journal papers and conference proceedings. He is a senior member of OSA and SPIE.

**Christopher B. Raub** is an assistant professor in the Department of Biomedical Engineering at CUA. His current research interests are in quantitative polarized light microscopy, and tissue microstructural and biochemical characterization from endogenous optical signals. He is a member of the Orthopedic Research and Biomedical Engineering Societies (ORS and BMES).